Internal and External Reconnection in a Series of Homologous Solar Flares

Alphonse C. Sterling[1] and Ronald L. Moore

Marshall Space Flight Center, SD50/Space Science Department, Huntsville, AL 35812

To appear in the Journal of Geophysical Research
(Accepted: July 17, 2000).

[1]NRC—MSFC Research Associate.

Abstract

Using data from the Extreme Ultraviolet Telescope (EIT) on *SOHO* and the Soft X-ray Telescope (SXT) on *Yohkoh*, we examine a series of morphologically homologous solar flares occurring in NOAA AR 8210 over May 1—2, 1998. An emerging flux region (EFR) impacted against a sunspot to the west and next to a coronal hole to the east is the source of the repeated flaring. An SXT sigmoid parallels the EFR's neutral line at the site of the initial flaring in soft X-rays. In EIT, each flaring episode begins with the formation of a crinkle pattern external to the EFR. These *EIT crinkles* move out from, and then fade in toward, the EFR with velocities ~ 20 km s^{-1}. A shrinking and expansion of the width of the coronal hole coincides with the crinkle activity, and generation and evolution of a postflare loop system begins near the time of crinkle formation. Using a schematic based on magnetograms of the region, we suggest that these observations are consistent with the standard reconnection-based model for solar eruptions, but modified by the presence of the additional magnetic fields of the sunspot and coronal hole. In the schematic, *internal reconnection* begins inside of the EFR-associated fields, unleashing a flare, postflare loops, and a CME. *External reconnection,* first occurring between the escaping CME and the coronal hole field, and second occurring between fields formed as a result of the first external reconnection, results in the EIT crinkles and changes in the coronal hole boundary. By the end of the second external reconnection, the initial setup is reinstated; thus the sequence can repeat, resulting in morphologically homologous eruptions. Our inferred magnetic topology is similar to that suggested in the "breakout model" of eruptions [*Antiochos,* 1998], although we cannot determine if our eruptions are released primarily by the breakout mechanism (external reconnection) or, alternatively, are released primarily by the internal reconnection.

1 Introduction

Largely based on results from the *Skylab* and *SMM* missions in the 1970's and early 1980's, a standard picture for solar flares and associated initiation of coronal mass ejections (CMEs) has emerged. In this picture, initially a filament or filament channel lies embedded in a canopy of overlaying magnetic field; the entire system can be represented by a single sheared arcade, with the lowest "core" fields the most sheared and the higher fields less sheared. Some process, such as reconnection or an instability, causes the core fields to erupt, displacing and stretching out the overlying field lines. As the eruption proceeds, the stretched field lines re-close via reconnection beneath the erupting filament. These reconnecting loops generate the intense soft X-ray emission of the flare, while the locations where these loops meet the photosphere are sources for the Hα ribbons and hard X-ray emission. These ideas have been developed by many workers over the years [e.g., *Hirayama,* 1974; *Kopp and Pneuman,* 1976; *Moore and LaBonte,* 1980; *Moore et al.,* 1991]. Observations from the *Yohkoh* satellite support various aspects of this model [e.g., *Masuda et al.,* 1994; *Shibata et al.,* 1995; *Forbes and Acton,* 1996; *Tsuneta,* 1997; *van Driel-Gesztelyi et al.,* 1997].

S-shaped or inverse S-shaped sigmoid structures seen with *Yohkoh*'s soft X-ray telescope (SXT) [e.g., *Rust and Kumar,* 1996; *Canfield, Hudson, and McKenzie,* 1999; *Gibson and Low,* 2000; *Sterling,* [2000] reviews recent observations] also fit into the standard picture; such "sigmoids" may represent a core field or flux rope which erupts. Initially the sigmoid

(sometimes associated with a filament) overlies a photospheric magnetic neutral line, with the ends of the sigmoid rooted in opposite polarity regions on either side of the neutral line. After eruption, an arcade of postflare loops, sometimes appearing cusp-shaped in SXT, overlies the location where the sigmoid was located [e.g., *Zarro et al.,* 1999; *Sterling et al.,* 2000].

Despite the apparent success of the the standard flare model, there have been challenges to its depiction of flares in terms of a fundamentally bipolar mechanism (a single sheared arcade), with some workers suggesting that a more complex magnetic field topology is vital (e.g., *Antiochos,* 1998; *Uchida et al.,* 1999), or that the entire scenario must be reconsidered (e.g., *Feldman and Seely,* 1995; *Hudson and Khan,* 1997). Therefore, it is necessary to test repeatedly the standard model against real data before concluding that the model actually correctly describes flares. In this paper we examine a series of flares occurring in NOAA active region 8210, which was on the solar disk in April and May 1998. Observations from SXT, and from the Extreme Ultra-Violet Imaging Telescope (EIT) on the *SOHO* satellite indicate that a number of these flares had a very similar appearance, that is, they were "morphologically homologous." Unlike the idealized geometry of the standard model outlined above, these eruptions occurred in a more complex magnetic environment, with an emerging flux region (EFR) sandwiched between the strong fields of a sunspot to the West and a weak, open, coronal hole-like field to the East. With each eruption, a distinctive, "crinkle"-like pattern of emission appears in EIT in regions separated from the main flaring location. Changes in the appearance of the coronal hole accompany the evolution of this crinkle pattern and the development of post-flare loop systems. We discuss EIT and SXT observations of flares from this region occurring on 1998 May 1—2, and attempt to interpret these observations in terms of the standard flare model. We will find that the standard flare model can schematically explain our observations. But in so doing we will also show evidence for reconnection occurring internal and external to the primary flaring region, indicating that a more complex magnetic geometry than generally assumed in the standard model played a role in the dynamics in this case.

2 Data and Instruments

We primarily use *SOHO* EIT data in our analysis. EIT [*Delaboudiniere et al.,* 1995] produces full-Sun images with a $2.6''$ pixels in four EUV wavelength bands, each covering a narrow wavelength range sensitive to the lower corona. We use the 195 Å Fe XII filter, which has the best time cadence among the EIT filters for the events of interest. It observes coronal plasmas with a narrow-band response peaked at approximately 1.5 MK. Most of the EIT images we examined for this study have exposure durations of 5 or 12 s. *Yohkoh*'s SXT [*Tsuneta et al.,* 1991] produces broad-band SXR images with a CCD camera with $2.5''$-pixels. It effectively detects plasma emissions $\gtrsim$2—3 MK by utilizing filters approximately spanning wavelengths of 3—45 Å. SXT coverage is interrupted by a satellite day-night cycle, while EIT coverage is essentially uninterrupted since *SOHO* is located at the L1 Lagrangian point. We also use magnetograms with $2.0''$-pixels obtained from the *SOHO* Michelson Doppler Imager [MDI; *Scherrer et al.,* 1995] in our analysis.

AR 8210 appeared on the solar disk in late April 1998, and was near disk center on May 1—2. It produced many flares, including a *GOES* X1.1–class event near 13:30 UT on May

2, 1998. We have examined in detail a continuous, 24 hour movie synthesized from EIT 195 Å images extending from 15 UT on May 1, 1998, and we augment this with full-frame image data from SXT throughout the time period. Figure 1 shows soft X-ray fluxes from the *GOES* satellite for the times covered, with the corresponding times of *Yohkoh* spacecraft night denoted by the hashed regions. These data show a number of events over the time period. We have found that the events near 18 UT and 23 UT on 1 May, and the event near 5 UT on 2 May have a close resemblance to each other in the EIT data. That is, they are morphologically homologous. The X flare also originated in AR 8210, but from a different location than the homologous set. We discuss the homologous events in detail in the following Sections.

3 Event Near 23 UT

We first discuss in detail SXT and EIT observations of the *GOES* M1 flare beginning near 22:15 UT and peaking near 23:00 UT in *GOES* soft X-rays (Fig. 1). We will then consider the other flares in the morphologically homologous series in § 4.

3.1 SXT Observations

Figure 2 shows SXT images of the region at various times during this event. These are subframes of SXT full-frame desaturated (SFD) images, which are created by combining images from short and long exposures in order to improve dynamic range. North is up and West is to the right in these and all other images of the paper.

The grey-scale images in Figures 2b and 2d are identical to those of Figures 2a and 2c, respectively, but overlaid with a magnetogram from MDI, with white and black indicating negative and positive polarities, respectively. This magnetogram shows a negative-polarity sunspot in the northwest, and a positive-polarity region butted up against this sunspot just to the southeast of the spot. Examination of MDI and Kitt Peak magnetograms from earlier times indicate that this positive flux is part of a newly emerging flux region (EFR), the negative polarity for which is lodged next to or inside the sunspot itself. White-light images indicate that the EFR itself is a delta-spot, which is impacted against the older, larger sunspot. Further to the east is a largely negative-polarity channel which outlines a region of more opened, coronal hole-like fields; this is best seen in Figure 2f, where fainter features are visible than in the other images. Figure 2a shows a bright sigmoid, surrounded by an anemone-type active region [*Shibata et al.,* 1994]. Figure 2b indicates that the body of this sigmoid does not overlay the magnetic neutral line, as sigmoids usually do [e.g., *Sterling et al.,* 2000; *Sterling,* 2000]. It does, however, roughly parallel the neutral line, and we suspect that it is displaced to the east in response to distortions in the overall topology of the region due the strong field rooted in the sunspot.

Figure 2c shows that the soft X-ray morphology of the region has changed markedly at the initiation of the eruption, corresponding to the time of rapid increase in *GOES* intensity (Fig. 1). Figure 2d shows extensions of the anemone region out into the coronal hole region, with a prominent extension to the southeast anchored in a negative-polarity patch. Following this, the central portion of the erupting region near the location of the sigmoid evolves into a series of bright postflare loops running normal to the orientation of

the body of the sigmoid; Figure 2e shows these loops after they have dimmed substantially. These observations mimic the basic properties of sigmoid evolution with time in eruptive flares seen in SXT, with a sigmoid typically tracing a neutral line giving way to a postflare loop system oriented normal to the neutral line [e.g., *Rust and Kumar,* 1996; *Sterling et al.,* 2000]. In this case, after the postflare loops fade, Figure 2f shows that a sigmoid again appears very near the location of the original sigmoid; we discuss this reappearance further in § 4.

3.2 EIT Observations

Figure 3 shows the same region in EUV taken with the 195 Å EIT filter. Figures 3d and 3j show overlays of the MDI magnetogram (the same one used in Figs. 2b and 2d) on the images in Figures 3c and 3i, respectively. Figure 3a is at a time just prior to the start of the soft X-ray intensity increase, the peak of which occurs near the time of the image in Figure 3f (cf. Fig. 1). Eruption-related changes become evident by the time of Figure 3b, where a patchy pattern of emission, which we call *EIT crinkles,* begins to intrude into the coronal hole region. These crinkles are more prevalent in the following frames. Figures 3b—3e show a prominent crinkle in the southeast (indicated by the arrow in Fig. 3b), with Figure 3d showing that this crinkle occurs in the negative-polarity patch on the east side of the coronal hole. This is the same flux patch to which a feature seen by SXT extends in Figure 2d, and therefore the EUV crinkles appear to be footpoints of extended loops seen in soft X-rays. This particular patch smoothes out in Figures 3f and 3g, indicating that these loops cool to EUV temperatures over about 40 min. After the development of the crinkles, a prominent set of postflare loops develops, showing apparent motion away from the flare source region in and after Figure 3g. These loops are beginning to fade significantly by the time of Figure 3l. Figure 3l is similar in appearance to Figure 3a, just as the soft X-ray images near the same respective times (Figs. 2f and 2a) are very similar in appearance.

Our movie made from EIT images[1], only a subset of which are displayed in Figure 3, shows that the crinkles appear to move away from the source of the eruption initially (approximately over times between 21:48 UT and 22:23 UT), and then retreat back in toward the eruption site at later times (approximately 23:14 UT and 23:50 UT). During the retraction, the crinkles generally take on a smoother appearance, consistent with them being the footpoints of loops having cooled to EUV-emitting temperatures. If these represent actual motions, the corresponding velocities are 15—20 km s^{-1} for both extension and retraction, although an absolute determination is difficult since a front to the crinkle pattern is not well defined. In contrast, the postflare loops evolve with an apparent velocity of only about 2.5 km s^{-1} between 00:03 UT and 01:17 UT on May 2, 1998. These values are not atypical of those seen in studies of postflare loops [e.g., *Bruzek,* 1964; *van Driel-Gesztelyi et al.,* 1997].

Figure 3 also shows changes with time in the width of the coronal hole region. For example, the coronal hole region is nearly completely filled with faint emission in Figure 3f, whereas it is a dark channel in Figure 3i. At this later time the minimum width of the

[1]An MPEG version of the EIT movie is available via Web browser or via Anonymous FTP from ftp://kosmos.agu.org, directory "apend" (Username = "anonymous", Password = "guest"); subdirectories in the ftp site are arranged by paper number. Information on searching electronic supplements is found at http://www.agu.org/pubs/esupp_about.html.

hole, measured across the sharp intensity boundaries at a latitude of -300 S (vertical axis in Figure 3i), is 15,000—20,000 km. Figure 3j indicates that, at its widest, the west side of the coronal hole is well-marked by a line of moderately strong negative-polarity patches. A lobe of the anemone region determines this boundary. The eastern boundary of the coronal hole is also near negative-polarity patches, although those patches do not mark the boundary as well as the western side in this magnetogram (the weakest contours are 25 G).

We also saw coronal hole-boundary size changes that appear to result from the late-stage evolution of postflare loops, but this seems to be distinct from the changes noted above.

4 Homologous Events

As noted in § 2, inspection of an EIT movie covering the time period of Figure 1 indicates that the events near 18 UT, 23 UT (both on May 1, 1998), and 5 UT (May 2) have a very similar appearance. We show this in Figure 4, with one row of two panels for each of the three events. Figures 4a, 4c, and 4e respectively show the region at times in the three events when EIT crinkles are visible and the coronal hole width is relatively narrow. Figures 4b, 4d, and 4f show the regions for the same respective events at a time after the crinkles have retracted, postflare loops are bright and growing, and the coronal hole is near its maximum width. Although there are some differences in the details, the striking similarities in the images suggest to us that these are morphologically homologous events. We also found that the SXT sigmoid feature reappears prior to each crinkle episode. Two examples of this can be seen by comparing Figures 2 and 4: the sigmoids of Figures 2a and 2f precede the crinkle episodes of Figures 4c and 4e, respectively. This pattern of repetition precedes the first event we examined in detail (postflare loops from an earlier episode are evolving outward at the start of the time period covered in Fig. 1), and likely extends beyond that of our third event.

We can identify portions of the sigmoid next to the postflare loops very shortly after the (relatively low-intensity) eruption near 18 UT. Therefore, we suspect that the sigmoid is present during the entire time period of Figure 1, but cannot be seen near the time of intensity peaks since it is much dimmer than the flaring loops. It is likely that only a portion of the sigmoid erupted into the flare, while the remainder is available for future eruptions, perhaps augmented by newly-emerging flux between outbursts.

These events are not homologous in their *GOES* soft X-ray profiles; the differences may be a result of an inability to reinstate the exact character of the active region prior to each event. There is also some variation in the properties of the events seen in EIT regarding the velocities of the crinkles and postflare loops; these properties are summarized in Table 1.

5 Schematic Interpretation

Various aspects of our observations of AR 8210 are not readily explainable with a single dipole, single neutral line eruption model such as the standard model discussed in § 1. These aspects include the relationship between the anemone structure of the AR and the sigmoid, the appearance and the dynamics of the EIT crinkles, and the variations in the width of the coronal hole. In this Section we will demonstrate schematically that the standard model

can provide a plausible explanation for our findings, provided we consider the magnetic environment that the eruptions occur in.

Figure 5a shows a 2-D cross-section of the basic magnetic setup that exists prior to the onset of flare or crinkle activity, corresponding to, e.g., Figure 2a in soft X-rays and Figure 3a in EUV. From the magnetogram in Figures 2b, 2d, 3d, and 3j, we qualitatively infer the geometry of the the magnetic field to be as depicted in Figure 5a, with a negative-polarity sunspot on the right side, a negative-polarity coronal hole on the left side, and an emerging flux region (EFR) in the middle. We suggest that a flux rope is lodged near the base of the EFR, based on the location of the sigmoid in soft X-rays. Because of the configuration of the magnetic polarities in the photosphere, loops forming an anemone lobe connect the plus of the EFR with the minus of the coronal hole. Due to the strong field of the sunspot, the field lines of the EFR are forced to lean over toward the left; this is in agreement with our observation that the sigmoid is offset to the east of the magnetic neutral line (Fig. 2b). As depicted here, the sigmoid, EFR, and sunspot form a delta-spot, which is a complicated structure in 3-D [examples of recent models of delta-spots include *Fan et al.,* 1999; *Linton et al.,* 1999].

Figure 5b shows the situation when a flux rope and surrounding fields erupt upward and are guided toward the left by the sunspot field lines (we discuss possible causes for the eruption in § 6). Other flux ropes remain behind, making up the unerupted portion of the sigmoid. "External reconnections," i.e., reconnections external to the erupting EFR-related fields, occur between the erupting arcade over the flux rope and the coronal hole fields in the region of the clear rectangular box in the figure. This external reconnection leads to two "reconnection products," indicated by dashed lines in the figure. One of these is a dashed line above the clear rectangular box (this would be an open field line against the sunspot field), and the second is the dashed line below that box, extending over the anemone lobe to the left of the EFR (a closed field line). These reconnections thus eat away at the fields of the coronal hole, replacing them with an inflated anemone lobe and newly-reconnected open field lines. Each reconnection would be associated with an energy release resulting in heating of the anemone field lines so that they are bright in soft X-rays. This corresponds to the SXT image in Figure 2c, where new loops are seen extending from the sigmoid region to the far side of the coronal hole prior to the main soft X-ray flux increase (cf. Fig. 1). Footpoints of the newly-formed loops would respond to the impulsive deposition of energy by brightening in EUV, forming the EIT crinkles. These crinkles would move outward (to the left in Figure 5) with time as the reconnection progresses.

Figure 5b also shows that in addition to this external reconnection, we can expect "internal reconnection," i.e., internal to the erupting fields, to occur in association with a flare generated by the standard reconnection picture. This internal reconnection occurs in the region indicated by the shaded rectangular box, and results in two additional reconnection products, indicated by dashed lines in the figure; these are new fields surrounding the outward-moving flux rope, and new flare loops (which will evolve as postflare loops) at low altitudes. This explains the occurrence of the flare nearly simultaneous with or just after the appearance of the crinkles.

Figure 5c shows the situation after most or all of the coronal hole field has been eaten away. The flux rope, continuing to be wrapped in additional field by internal reconnection, now escapes into space and becomes a CME. Internal reconnection also continues to feed

the growth of the flare and postflare loop system near the site of the EFR. At this point the coronal hole width is near a minimum and the EIT crinkles have reached their maximum extent, corresponding to Figures 3f and 3g. After the last field lines of the arcade over the flux rope pinch off from the EFR, the oppositely-directed field lines of the inflated anemone lobe and the sunspot can come into contact with each other, and initiate a new series of reconnections (in three dimensions, the lobe and sunspot reconnection may begin before the legs of the flux rope have completely separated from the EFR).

Figure 5d shows the consequences of these new reconnections. Two reconnection products result from each episode, indicated by the dashed lines in the figure. One forms a new loop over the EFR, while the other forms an open field line. Consequences are that the anemone lobe shrinks and the coronal hole reforms. Associated with the reconnections leading to the shrinking anemone lobe will be retracting EIT crinkles, approximately corresponding to Figures 3h and 3i. As this continues, the initial setup (Fig. 5a) is reinstated, as in Figures 2f and 3l. Eruption of one of the remaining core flux tubes (or a newly-emerged one) will result in a repetition of the sequence. Newly emerging flux may increase the flux in the sigmoid, perhaps abetting the eruption.

It is interesting to compare the amount of magnetic flux in the EFR with that in the coronal hole that is potentially available to reconnect with the EFR fields. For the coronal hole and surrounding regions we use a rectangular region approximately defined by longitudes -60 — +50 arcseconds, and latitudes -150 — -390 arcseconds in the magnetogram as shown in Figures 2b and 3d. Totaling the negative flux of magnitude greater than 25 G (about the noise level in the magnetogram), we find about -4.6×10^{20} Mx in the region. For the positive flux in the EFR, we use a region roughly the shape of the positive-flux contour in Figures 2b and 3d, approximately bordered by longitudes +50 — +130 arcseconds, and latitudes -200 — -290 arcseconds. For this region, summing the positive flux of greater than 25 G yields about 2.4×10^{21} Mx. Thus the intense positive flux in the EFR dominates the weaker negative flux in the coronal hole and surrounding regions by approximately a factor of five. This means that, according to our scenario, only about one-fifth of the erupting flux is potentially available for external reconnection as the flux rope escapes (Figs. 5b and 5c), and for the recovery external reconnection (Fig. 5d). Probably less than 100% of the negative flux is actually involved in these reconnections, however. We also have not investigated flux changes with time, e.g., due to emergence of new flux.

This picture, then, allows us to explain the primary features discussed in § 3 and § 4, namely the appearance of the anemone lobe, the appearance of and the dynamic motions of the EIT crinkles, the timing of the appearance of the crinkles and the soft X-ray flare, the corresponding changes in the width of the coronal hole, and the ability of the region to produce morphologically homologous eruptions.

6 Discussion

We have found that the standard reconnection picture for solar flares is able to explain many of the observed features of AR 8210, provided that we model the system as a bipolar EFR lodged between a sunspot on one side and a coronal hole on the other side. The key point in explaining the observations is that an initial eruption of a low-lying core field associated with the soft X-ray sigmoid is followed by a progression of internal and external magnetic

reconnection episodes. Internal reconnections, i.e., reconnection among the erupting field lines only, result in enhancements to the outward-moving flux rope and initiation of the solar flare followed by a series of postflare loops; these internal-reconnection aspects of the evolution are the same as those described by the standard reconnection flare picture discussed in § 1. External reconnections occur between the ejected fields wrapped over the flux rope and the surrounding coronal hole fields early on, and then between the anemone fields and the newly-reconnected open field lines (next to the sunspot fields) after the field wrapping the flux rope pinches off as a CME from the flare-associated fields below. For the external reconnection, we envision a mechanism discussed (and simulated to some extent) in *Antiochos,* [1998], whereby oppositely-directed field lines push against each other until a very narrow current sheet forms and reconnection begins at null points. *Priest,* [1982] and *Forbes and Priest,* [2000] give overviews of magnetic reconnection.

Our schematic interpretation of activity in this region can naturally explain the tendency for morphologically homologous flaring, since the initial setup is reinstated following the completion of the eruption; with this, we are addressing one of the objections to reconnection-based flare models raised by *Hudson and Khan,* [1997], who pointed out difficulties with such models explaining homologous flares. Our scenario, however, does not specify the mechanism that initiates each new eruption.

We suggest that the EIT crinkle pattern and its time evolution are evidence for the external reconnection. We also expect external reconnections between the erupting flux rope and the coronal hole field lines in Figure 5b to result in the generation of high-speed electrons and associated Type III radio bursts along the newly-reconnected open field lines (the dashed open field line above the clear rectangle in Fig. 5b). We do in fact see Type III activity in 25—2500 MHz HiRAS data from the Hiraiso Solar Terrestrial Research Center (Japan) for the 23 UT May 1 event and the 5 UT May 2 event (no HiRAS data are available for the 18 UT May 1 event).

We have found the crinkle velocities to be about 20 km s^{-1} both when they are extending and when they are retracting. In our schematic view, these velocities should be related to the velocity of the ejecting flux rope and the rate of recovery reconnection in the aftermath of the ejection. Moreover, from Figures 5b and 5c, we expect the velocities of the growing crinkles projected on the surface to be no greater than that of the escaping flux rope. CMEs have velocities ranging from a few tens of km s^{-1} to about 2000 km s^{-1} [e.g., *Howard et al.,* 1985; *Hundhausen, Burkepile, and St. Cyr* 1994]. Soft X-ray ejections, some of which are likely to be associated with CMEs, have also been seen in SXT data. These features have velocities of one hundred to several hundred km s^{-1} [*Shibata et al.,* 1995; *Ohyama and Shibata,* 1997, 1998; *Tsuneta,* 1997; *Nitta and Akiyama,* 1999].

It is not unreasonable that the observed crinkle velocities are lower than the expected velocities of the flux rope leading to CMEs. One reason for this could be that the field lines of the coronal hole spread out substantially between the photosphere and the locations where they reconnect with the escaping flux rope. In that case, over a given time period, the distance over which the external reconnections occur would be much larger than the distance over which the crinkles form at the feet of the coronal hole field lines. This could explain a lower velocity of the crinkles than that expected of the flux rope, but we do not have any evidence to support this idea and hence it has to be regarded as speculation. An actual potential field calculation from the magnetogram may be able to address this

possibility in more detail.

Another possibility is that the crinkle dynamics occur before the fastest motion of the SXT plasmoids. *Ohyama and Shibata,* [1997] found a plasmoid rise velocity ~ 10 km s^{-1} prior to the hard X-ray intensity peak of the flare they observed. Light curves from the Hard X-ray Telescope (HXT) on *Yohkoh* peak at about 22:45 UT for our second event on May 1, 1998, which is after the initial crinkle activity for that event. For that same event, the first EIT crinkles appear in the image at 22:05 UT, while the increase in the *GOES* flux of Fig. 1 begins at about 22:15 UT. Therefore our velocities of about 20 km s^{-1} may be associated with the preflare (i.e., pre-hard X-ray burst) feature observed by *Ohyama and Shibata,* [1997], rather than the faster moving SXT plasmoid features seen at later times.

Our schematic description does not address the actual cause of the eruptions leading to the repeated activity in AR 8210. One possibility is that the driving source operates at a low altitude, specifically, in the vicinity of the soft X-ray sigmoid and the site of the initial internal reconnection. This could be due to instabilities brought on by driving motions in the photosphere acting on flux tubes or from the emergence of new flux tubes [e.g., *Sturrock,* 1989; *Forbes and Priest,* 1995; *Chen,* 1996; *Rust and Kumar,* 1996; *Moore et al.,* 1997; *Wu, Guo, and Dryer,* 1997; *Amari et al.,* 2000]. Another alternative is the eruptions result from reconnection of field lines near the sigmoid [e.g., *Moore and LaBonte,* 1980; *Sturrock,* 1989]; this mechanism is sometimes referred to as "tether cutting."

Antiochos, [1998] and *Antiochos, DeVore, and Klimchuk,* [1999] have suggested a different type of trigger mechanism, one which relies on a more complicated magnetic geometry than a single bipole. In their view, a broad system of overlying fields prevents an emerging bipole from escaping into space. Thus the overlying fields restrain the emerging flux, and stress builds up in the form of current sheets at the boundaries between the restraining fields and the emerging flux pushing upward. Slow reconnection ensues at the sites of the current sheets, eroding the overlying fields. When enough of the restraining field is eroded away, the underlying emerging fields breakout of the system, ejecting a CME and (perhaps) forming a flare. Our inferred magnetic topology in AR 8210 is consistent with this "breakout model." Viewed in terms of that model, the fields associated with the EFR in Figure 5a would not reconnect with the coronal hole fields until sufficient stress builds up and the current sheet at the boundary between the flux systems becomes large and thin. Once breakout occurs, the erupting flux tube would slip out between the sunspot fields and the remaining unreconnected coronal hole fields.

Based on the analysis we have presented in this paper, we are not able to determine whether the eruptions we observe are released by the external reconnection according to this breakout picture, or instead are released by internal reconnection lower down in the region of the sigmoid, or are initiated by some other mechanism. Our observations do, however, present strong evidence for external reconnection between erupting fields and surrounding fields near the time of eruption. Thus we can only conclude that, in this case, a breakout-model magnetic topology appears to be present.

In conclusion, the standard reconnection picture can explain the observed repetitive eruptions, EIT crinkles, and other features, given an appropriate magnetic topology. Moreover, the inferred magnetic topology based on photospheric magnetogram data is similar to the setup proposed by Antiochos for the breakout model for solar eruptions. Examination of these data alone, however, is not adequate to establish if the eruptions in AR 8210 were

built up and released by the process suggested in the breakout model, or if the eruptions originate in the core-field region. Future studies should address whether the breakout magnetic topology is a general feature of erupting regions, perhaps with the surrounding fields only appearing very faint in cases that initially appear to be purely bipolar, or if tether cutting or some other mechanism is the responsible agent. High-resolution observations from the *TRACE* satellite and from the upcoming *Solar B* mission should be particularly useful in addressing these issues.

We thank A. Gary, K. Hori and H. S. Hudson for useful discussions. We also thank H. Hudson for assisting in directing our attention to this active region. This work was performed while A.C.S. held a National Research Council—NASA/MSFC Research Associateship.

References

Amari, T., Luciani, J. F., Mikic, Z., and Linker, J., A Twisted Flux Rope Model for Coronal Mass Ejections and Two-Ribbon Flares, ApJ *529,* L49—L52, 2000.

Antiochos, S. K., The Magnetic Topology of Solar Eruptions, ApJ *502,* L181—L184, 1998.

Antiochos, S. K., A Model for Solar Coronal Mass Ejections, ApJ *510,* 485—493, 1999.

Bruzek, A., On the Association Between Loop Prominences and Flares, *Solar Phys., 140,* 746—759, 1964.

Canfield, R. C., Hudson, H. S., McKenzie, D. E., Sigmoidal morphology and eruptive solar activity, *Geophys. Res. Lett., 26,* 627—630.

Chen, J., Theory of prominence eruption and propagation: Interplanetary consequences, *J. Geophys. Res., 101,* 27,499—27,519, 1996.

Delaboudiniere, J.-P. et al., EIT: Extreme-ultraviolet imaging telescope for the soho mission, *Solar Phys., 162,* 291—312, 1995.

Fan, Y., Zweibel, E. G., Linton, M. G., and Fisher, G. H., The Rise of Kink-unstable Magnetic Flux Tubes and the Origin of δ-Configuration Sunspots, ApJ, *521,* 460—477, 1999.

Feldman, U., and Seely, J. F., Relationship between Cold and Hot Post—Solar Flare Loops and the Impact on the Reconnection Flare Model, ApJ *450,* 902—906, 1995.

Forbes, T. G., and Priest, E. R., Photospheric Magnetic Field Evolution and Eruptive Flares, ApJ *446,* 377—389, 1995.

Forbes, T. G., Priest, E. R., *Magnetic Reconnection : Mhd Theory and Applications,* Cambridge Univ. Press., 2000.

Forbes, T. G., and Acton, L. W., Reconnection and Field Line Shrinkage in Solar Flares, ApJ *459,* 330—341, 1996.

Gibson, S. E., and Low, B. C., Three-dimensional and twisted: An MHD interpretation of on-disk observational characteristics of coronal mass ejections, *J. Geophys. Res.,* in press, 2000.

Hirayama, T., Theoretical Model of Flares and Prominences. I: Evaporating Flare Model, *Solar Phys., 34,* 323—338, 1974.

Howard, R. A., Sheeley, N. R., Jr., Michels, D. J., Koomen, M. J., Coronal mass ejections: 1979—1981. *J. Geophys. Res., 90,* 8173—8191, 1985.

Hudson, H. S., and Khan, J. I., Observational Problems for Flare Models Based on Large-Scale Magnetic Reconnection, in *Magnetic Reconnection in the Solar Atmosphere. ASP Conference Series, vol. 111,* edited by R. D. Bentley and J. T. Mariska, pp. 135—144, 1997.

Hundhausen, A. J., Burkepile, J. T., St. Cyr, O. C., Speeds of coronal mass ejections, SMM observations from 1980 and 1984-1989, *J. Geophys. Res., 99,* 6543—6552, 1994.

Kopp, R. A., and Pneuman, G. W., Magnetic reconnection in the corona and the loop prominence phenomenon, *Solar Phys., 50,* 85—98, 1976.

Linton, M. G., Fisher, G. H., Dahlburg, R. B., and Fan, Y., Relationship of the Multimode Kink Instability to delta-Spot Formation, ApJ, *522,* 1190-1205, 1999.

Masuda, S., Kosugi, T., Hara, H., Tsuneta, S., Ogawara, Y., A Loop-Top Hard X-Ray Source in a Compact Solar Flare as Evidence for Magnetic Reconnection, *Nature, 371,* 495—497, 1994.

Moore, R. L., LaBonte, B. J., The filament eruption in the 3B flare of July 29, 1973: onset and magnetic field configuration, in *Solar and interplanetary dynamics, IAU Symp. 91,* edited by M. Dryer and E. Tandberg-Hanssen, pp. 207—210, (Reidel, Boston), 1980.

Moore, R. L., Hagyard, M. J., Davis, J. M., Porter, J. G., The MSFC Vector Magnetograph, Eruptive Flares, and the Solar-A X-ray Images, in *Flare Physics in Solar Maximum 22,* edited by Y. Uchida, R. C. Canfield, T. Watanabe, and E. Hiei (Springer-Verlag:Berlin), pp. 324—329, 1991.

Moore, R. L., Schmieder, B., Hathaway, D. H., Tarbell, T. D., 3-d magnetic field configuration late in a large two-ribbon flare. *Solar Phys., 176,* 153—169, 1997.

Nitta, N., Akiyama, S., Relation between Flare-associated X-Ray Ejections and Coronal Mass Ejections, ApJ *525,* L57—L60, 1999.

Ohyama, M., and Shibata, K., Preflare Heating and Mass Motion in a Solar Flare Associated with Hot Plasma Ejection: 1993 November 11 C9.7 Flare, *Pub. Astro. Soc. Japan, 49,* 249—261, 1997.

Ohyama, M., and Shibata, K., X-Ray Plasma Ejection Associated with an Impulsive Flare on 1992 October 5: Physical Conditions of X-Ray Plasma Ejection, ApJ *499,* 934—944, 1998.

Priest, E. R., *Solar Magnetohydrodynamics,* Reidel, Dordrecht, 1982.

Rust, D., M., Kumar, A., Evidence for helically kinked magnetic flux ropes in solar eruptions, ApJ *464,* L199—L202, 1996.

Scherrer et al., The Solar Oscillations Investigation - Michelson Doppler Imager, *Solar Phys., 162,* 129—188, 1995.

Shibata, K., Nitta, N., Strong, K. T., Matsumoto, R., Yokoyama, T., Hirayama, T., Hudson, H., and Ogawara, Y., A gigantic coronal jet ejected from a compact active region in a coronal hole, ApJ *431,* L51, 1994.

Shibata, K., Masuda, S., Shimojo, M., Hara, H., Yokoyama, T., Tsuneta, S., Kosugi, T., Ogawara, Y., Hot-Plasma Ejections Associated with Compact-Loop Solar Flares, ApJ *451,* L83—L85, 1995.

Sterling, A. C., Sigmoid CME Source Regions at the Sun: Some Recent Results, *J. of Atmos. and Solar-Terrestrial Phys.,* in press, 2000.

Sterling, A., C., Hudson, H. S., Thompson, B. J., and Zarro, D. M., *Yohkoh* SXT and *SOHO* EIT Observations of "Sigmoid-to-Arcade" Evolution of Structures Associated

with Halo CMEs, ApJ in press, 2000.
Sturrock, P. A., The Role of Eruption in Solar Flares, *Solar Phys., 1212,* 387—397, 1989.
Tsuneta, S., et al., The soft X-ray telescope for the Solar-A mission, *Solar Phys., 136,* 37—67, 1991.
Tsuneta, S., Moving Plasmoid and Formation of the Neutral Sheet in a Solar Flare, ApJ *483,* 507—514, 1997.
Uchida, Y., Hirose, S., Cable, S., Morita, S., Torii, M., Uemura, S., Yamaguchi, T., A Quadruple Magnetic Source Model for Arcade Flares and X-Ray Arcade Formations outside Active Regions I. Dark Filament Suspension and the Magnetic Structure in the Pre-Event Regions, *Pub. of the Astro. Soc. of Japan, 51,* 553—563, 1999.
van Driel-Gesztelyi, L., Wiik, J. E., Schmieder, B., Tarbell, T., Kitai, R., Funakoshi, Y., Anwar, B., Post-Flare Loops of 26 June 1992 - IV. Formation and Expansion of Hot and Cool Loops, *Solar Phys., 174,* 151—162, 1997.
Wu, S. T., Guo, W. P., and Dryer, M., Dynamical Evolution of a Coronal Streamer—Flux Rope System: II. A Self-Consistent Non-Planar Magnetohydrodynamic Simulation, *Solar Phys., 170,* 265, 1997.
Zarro, D. M., Sterling, A. C., Thompson, B. J., Hudson, H. S., and Nitta, N., *SOHO* EIT Observations of Extreme-Ultraviolet "Dimming" Associated with a Halo Coronal Mass Ejection, ApJ *520,* L139—L142, 1999.

Captions

Figure 1. Soft X-ray light curves from the *GOES*–9 spacecraft covering the time period addressed in this study. Hashed areas represent times of *Yohkoh* spacecraft night. The three morphologically homologous events of this paper peak near 18 UT and 23 UT on May 1, and 5 UT on May 2, 1998. The X flare on May 2 occurred in a different location of AR 8210 than the three earlier events, and thus is not part of the morphologically homologous sequence.

Figure 2. Grey-scale images from *Yohkoh*'s SXT instrument, taken with the AlMg filter for (a) and (b), and the Al1.1 filter for (c)—(f). The images in (a) and (c) are repeated in (b) and (d), respectively, overlaid by positive (black) and negative (white) magnetogram contours of levels 25, 40, and 500 g from the *SOHO* MDI instrument, taken at 22:24 UT on May 1, 1998. Some of the extensions in (c) reach to locations of EIT crinkles seen in Fig. 4. In these and in all other images in this paper, North is up and West is to the right, and size scales are listed in arcseconds from solar-disk center.

Figure 3. Grey-scale images from *SOHO*'s EIT instrument, taken with the 195 Å Fe XII filter. The images in (c) and (i) are repeated in (d) and (j), respectively, overlaid by the same magnetogram contours as in Fig. 2. EIT crinkles appear in (b)—(g), with the arrow in (b) indicating a developing prominent crinkle.

Figure 4. Grey-scale images from *SOHO*'s EIT instrument, taken with the 195 Å Fe XII filter. Each row is from a different event in the morphologically homologous sequence discussed in the text. Panels on the left show each event at a time when the EIT crinkle

pattern is present and the coronal hole is near minimum width, and images on the right show each event after the crinkles have faded, postflare loops are evolving, and the coronal hole is near maximum width.

Figure 5. Schematic diagram depicting the suspected progression of events seen in Figs. 2 and 3. Lines represent magnetic field lines of negative (pointing downward) or positive (pointing upward) polarities. Dashed lines indicate new field lines about to be formed in a reconnection episode about to take place. To aid in clarity, some field lines are bold (closed field lines and flux-rope field lines), while others are thin (open fields and sunspot field lines). (a) A flux tube is lodged beneath an EFR, appearing as a sigmoid in soft X-rays. (b) A portion of the flux rope erupts and its envelope reconnects (external reconnection) with coronal hole fields, increasing the extent of the anemone lobe beneath it and producing EIT crinkles at the feet of the lobe. Much of the flux rope remains at the original location. Internal reconnection also occurs, augmenting the flux wrapping the flux rope, and causing a flare and postflare loops below via the standard reconnection flare model. (c) Virtually all of the coronal hole has been consumed by external reconnection. The erupting wrapped flux rope is about to escape as a CME, leaving a flare and growing postflare loops in its wake. (d) Reconnection (external reconnection) between the anemone lobe fields and the newly-reconnected open fields (i.e., fields like the uppermost dashed line in b) lead to a reformation of the coronal hole and the retraction of the anemone fields with retracting EIT crinkles at the base. After some time the situation is (a) is restored, and a new eruption will restart the cycle. In (b) and (d), clear rectangles indicate locations of ongoing external reconnection, and in (b) and (c) shaded rectangles indicate regions of the ongoing internal reconnections. Most energy is released in the internal reconnections, which result in the bulk of the soft and hard X-ray flare emissions.

Table 1: Properties of EIT Crinkles and Postflare Loops in Three Eruptions.

GOES Peak Time (UT)	Extension[a] (UT)	Retraction[a] (UT)	Velocity[a] (km s^{-1})	Loop Velocity[b] (km s^{-1})
17:57	17:09:53—17:26:57	17:59:32—18:17:53	20—30	4.3
22:54	21:48:03—22:22:53	23:13:58—23:49:57	15—20	2.5
05:00	04:18:55—04:53:39	05:52:48—07:17:33	$\gtrsim$20	4.8

[a] Values for EIT Crinkles (times approximate)
[b] Values for Postflare Loops

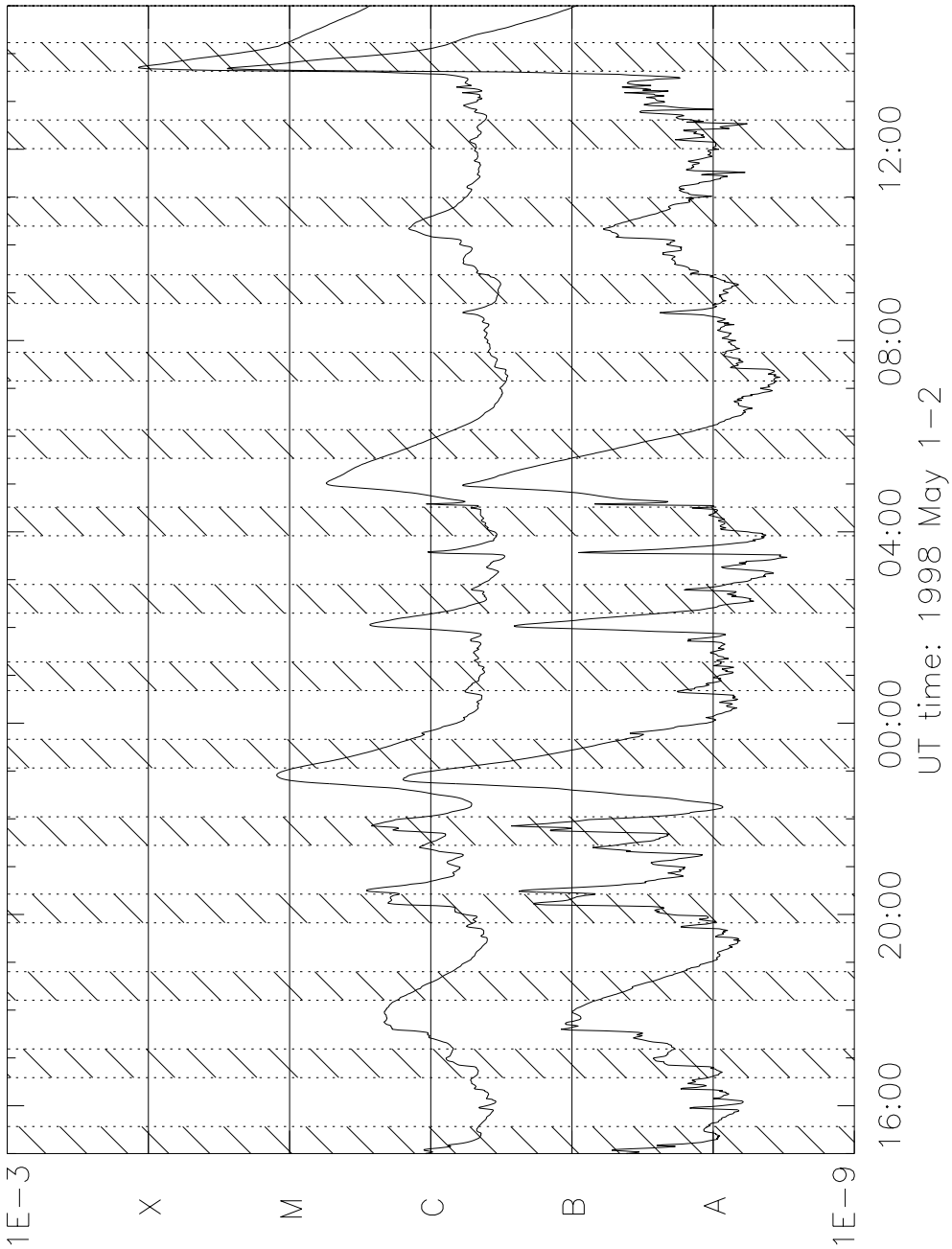
1E−3
X
M
C
B
A
1E−9
16:00
20:00
00:00
04:00
08:00
12:00
UT time: 1998 May 1−2

Figure 1:

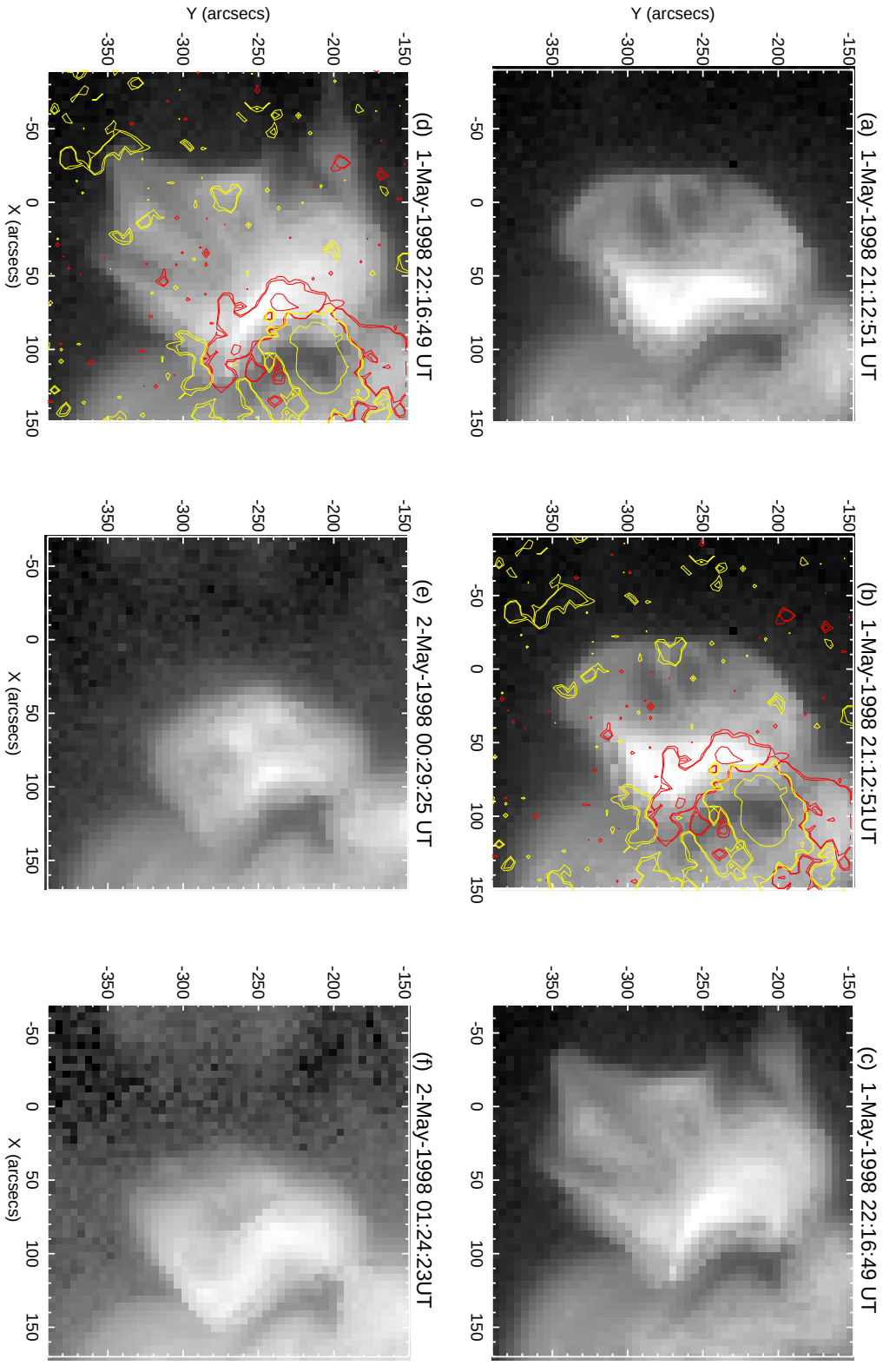
(a) 1-May-1998 21:12:51 UT
(b) 1-May-1998 21:12:51UT
(c) 1-May-1998 22:16:49 UT
(d) 1-May-1998 22:16:49 UT
(e) 2-May-1998 00:29:25 UT
(f) 2-May-1998 01:24:23UT
Y (arcsecs)
X (arcsecs)
-150
-200
-250
-300
-350
-50
0
50
100
150

Figure 2:

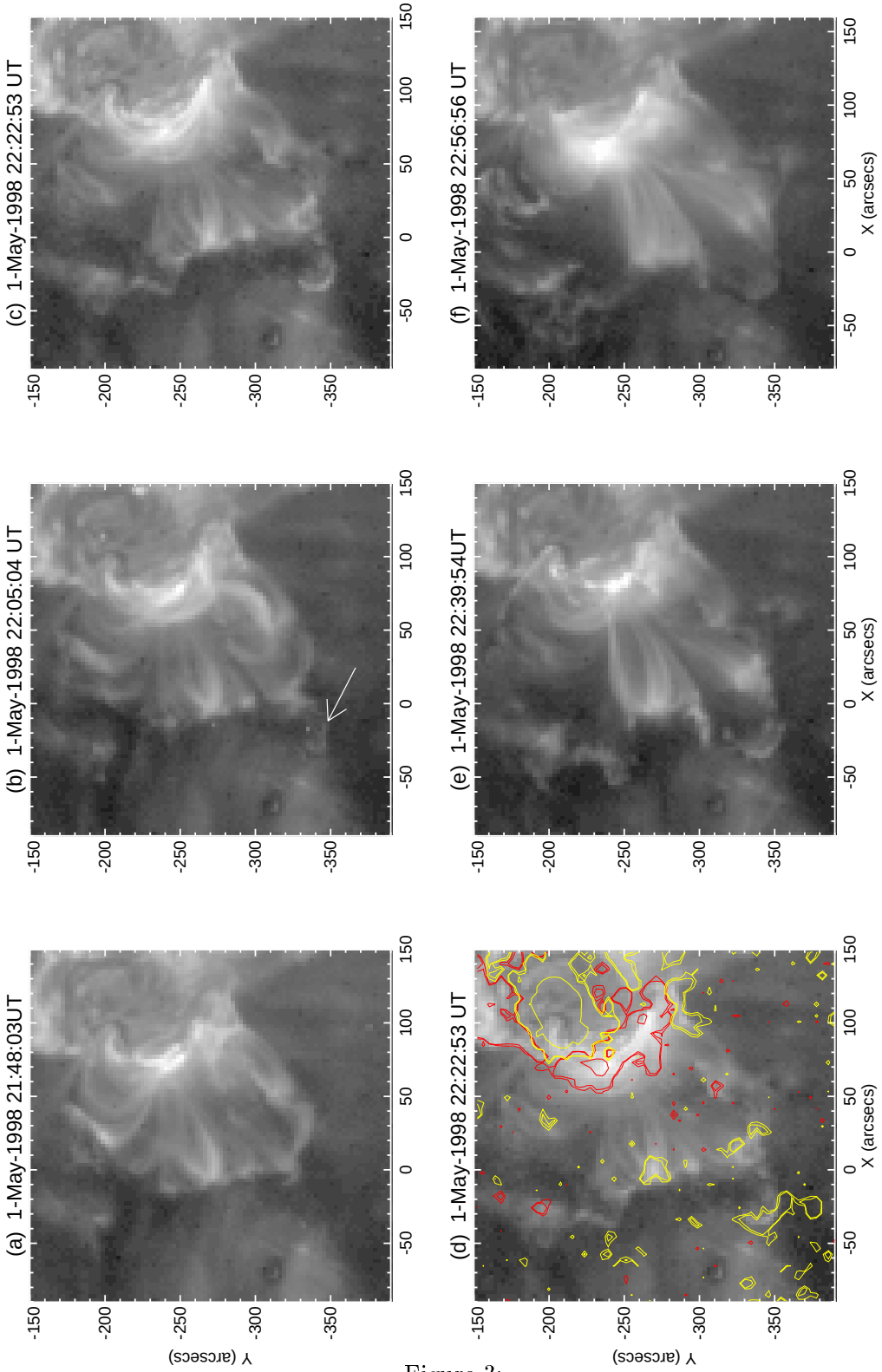
(a) 1-May-1998 21:48:03UT
(b) 1-May-1998 22:05:04 UT
(c) 1-May-1998 22:22:53 UT
(d) 1-May-1998 22:22:53 UT
(e) 1-May-1998 22:39:54UT
(f) 1-May-1998 22:56:56 UT
Y (arcsecs)
X (arcsecs)
-150
-200
-250
-300
-350
-50
0
50
100
150

Figure 3:

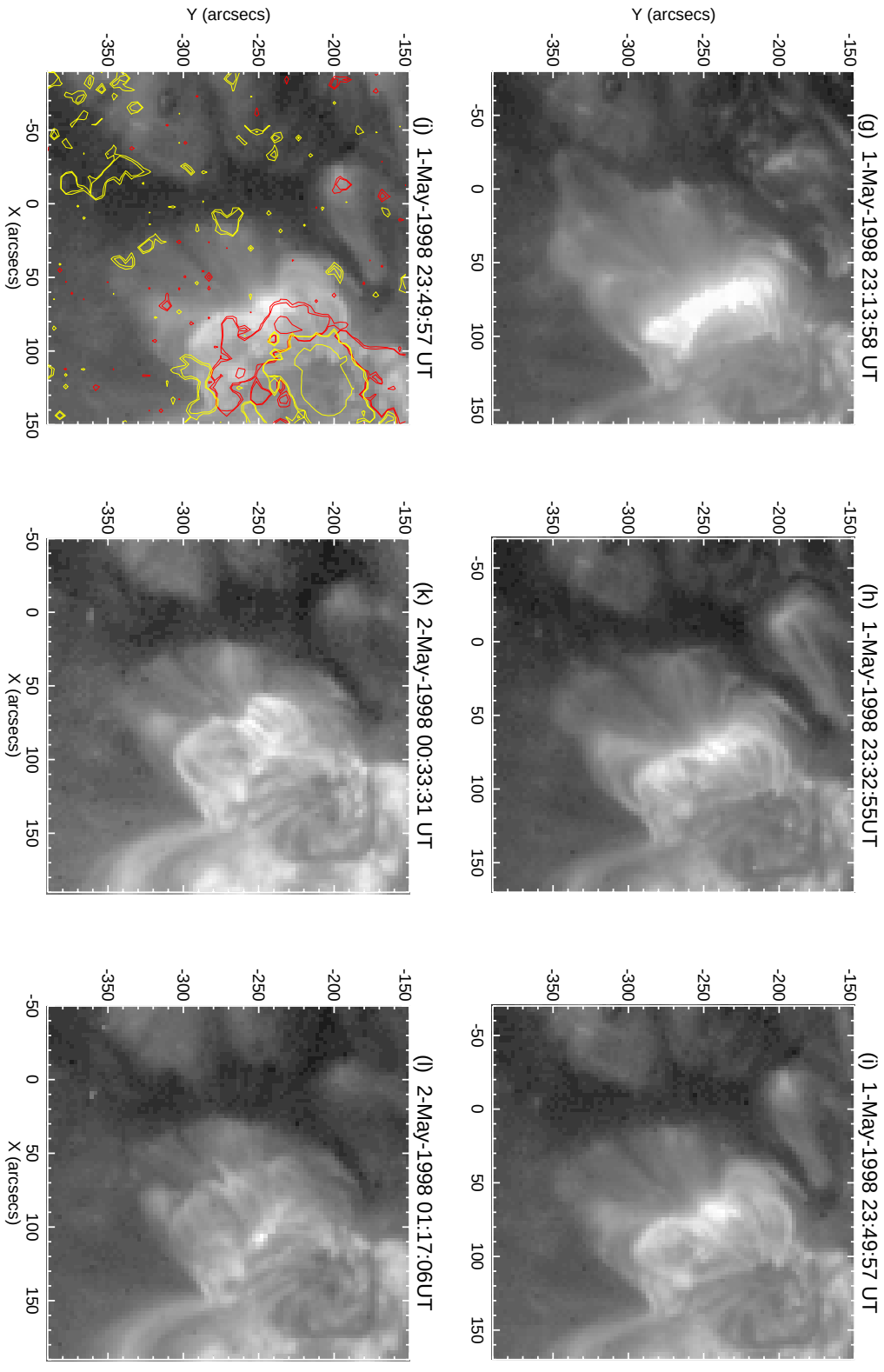

Figure 3: (Continued)

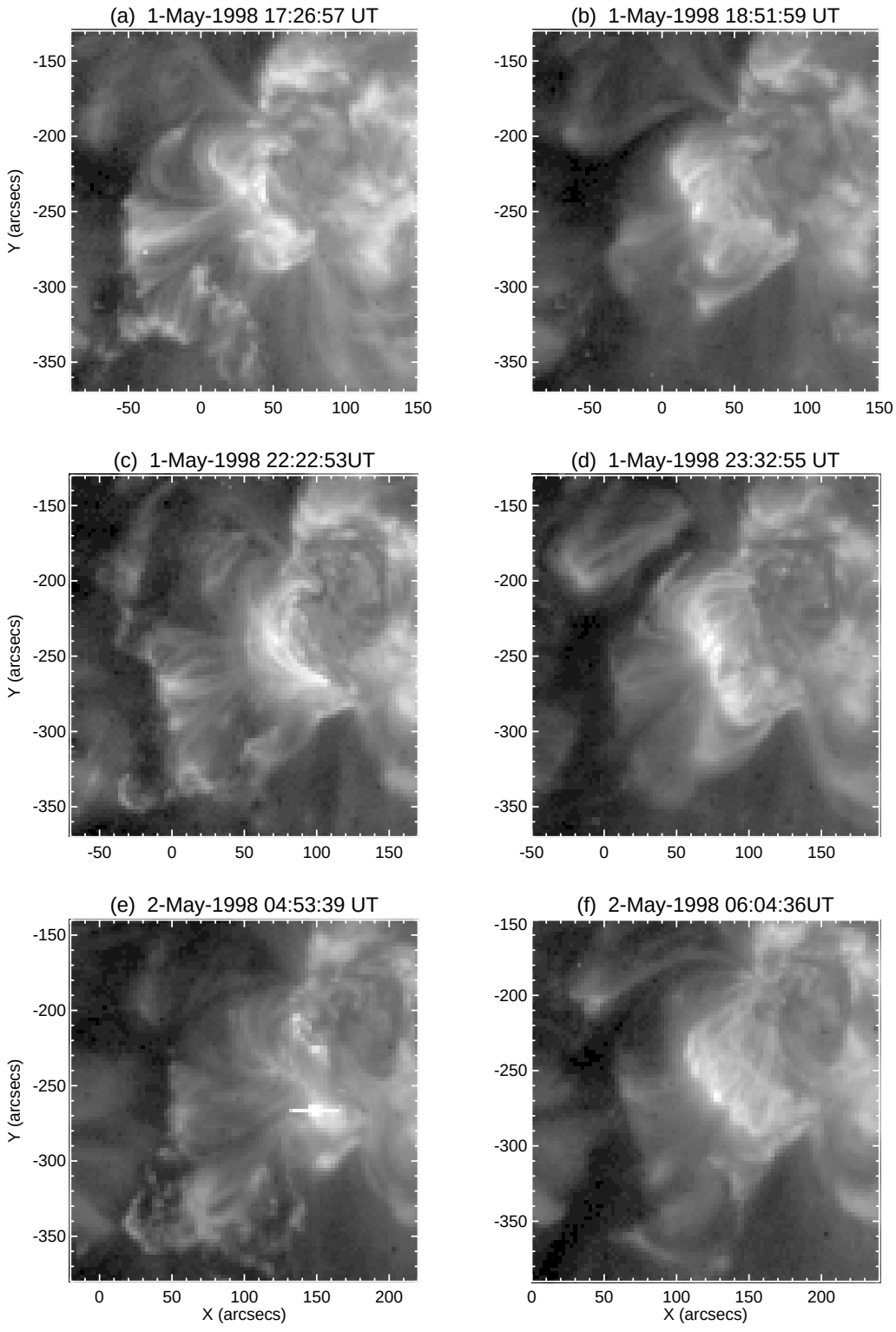
(a) 1-May-1998 17:26:57 UT
(b) 1-May-1998 18:51:59 UT
(c) 1-May-1998 22:22:53UT
(d) 1-May-1998 23:32:55 UT
(e) 2-May-1998 04:53:39 UT
(f) 2-May-1998 06:04:36UT
Y (arcsecs)
X (arcsecs)
-150
-200
-250
-300
-350
-50
0
50
100
150
200

Figure 4:

(a)
minus
Coronal Hole
plus
minus
EFR
minus
Sunspot
(b)
minus
Coronal Hole
plus
minus
EFR
minus
Sunspot
(c)
minus
plus
minus
EFR
minus
Sunspot
(d)
minus
Coronal Hole
plus
minus
EFR
minus
Sunspot

Figure 5: